Structure of the Membrane Reconstituted Transmembrane−Juxtamembrane Peptide EGFR(622−660) and Its Interaction with Ca^{2+}/Calmodulin†

Takeshi Sato,‡ Payal Pallavi,§ Urszula Golebiewska,§ Stuart McLaughlin,§ and Steven O. Smith*,‡

Department of Biochemistry and Cell Biology, Center for Structural Biology, and Department of Physiology and Biophysics, Stony Brook University, Stony Brook, New York 11794-5215

Received June 24, 2006; Revised Manuscript Received August 30, 2006

ABSTRACT: The transmembrane (TM) and juxtamembrane (JM) regions of the epidermal growth factor receptor (EGFR) couple ligand binding in the extracellular domain to activation of the kinase domain. Solid-state NMR and polarized FTIR measurements of peptides corresponding to the TM plus JM regions of EGFR (residues 622−660) reconstituted in model phospholipid membranes are presented to address the role of the short cytoplasmic JM sequence (residues 645−660) in regulating EGFR activity. We show that the TM domain is helical with a transition to non-helical structure at the TM−JM boundary. Fluorescence measurements indicate that the JM region of EGFR(622−660) binds to the membrane surface and that binding can be reversed by the addition of the complex of Ca^{2+} and calmodulin. Together these data support models suggesting the cytoplasmic JM region of EGFR plays an active role in regulating receptor activity.

The epidermal growth factor receptor (EGFR)[1] is a member of the ErbB family of receptor tyrosine kinases (RTKs). These receptors are cell-surface membrane proteins that mediate cell growth and differentiation. Their activity is tightly regulated by a variety of mechanisms including phosphorylation (*1*−*3*), dephosphorylation (*4*), membrane trafficking (*5*), and endocytosis (*6*). Mutations and deletions in the EGFR and other RTKs that result in constitutive receptor activity have been identified in a variety of human tumors (*7*, *8*), and there remains considerable interest in the mechanism(s) by which these receptors are activated and regulated.

Recent crystal structures of the extracellular domain of the EGFR with (*9*) and without (*10*) bound EGF provide a significant step forward in understanding the molecular details of the activation mechanism. EGF binding triggers a dramatic rearrangement of the four extracellular subdomains in each receptor monomer (Figure 1). The structural changes in the extracellular domain produce either dimerization (left to center in Figure 1) or rearrangement of pre-existing dimers (right to center in Figure 1). In most RTKs, ligand binding leads to phosphorylation of tyrosines in the activation loop within the intracellular kinase domain; the activation loop in the unphosphorylated receptor blocks the active site of the kinase. In contrast to this mechanism, an elegant recent report from the Kuriyan laboratory shows that the activation loop in the kinase domain of the EGFR is activated by an allosteric mechanism that results from the formation of an asymmetric kinase dimer (*11*, *12*). Other models seem unlikely in light of the Kuriyan study. For example, Ben-Tal and co-workers (*13*) proposed a model where a cluster of acidic residues (979−991) in the C-terminal tail of the EGFR kinase domain binds to a region of positive electrostatic potential in the kinase domain and inhibits it, while Aifa et al. (*14*, *15*) proposed a model where the same cluster of acidic residues binds to the JM region of an adjacent kinase to mediate dimerization and orient the C-terminal tail for phosphorylation and activation.

We have recently proposed a mechanism for the autoinhibition and activation of the EGFR/ErbB family (*16*) that relies on the presence of a flexible juxtamembrane (JM) region between the transmembrane (TM) and kinase domains. The model postulates that in the inactive receptor (Figure 1), the JM and kinase domains associate electrostatically with the negatively charged plasma membrane. The JM domain has a net positive charge, as does one face of the kinase domain. Dimerization or dimer rearrangement (Figure 1) is the first step in receptor activation and leads to a well documented (*3*) increase in the level of Ca^{2+} in the cytoplasm. Binding of intracellular Ca^{2+} to calmodulin allows the Ca^{2+}-calmodulin complex (with a −16 charge) to bind to the positively charged JM sequence of EGFR and triggers

† This work was supported by NIH-NSF instrumentation grants (S10 RR13889 and DBI-9977553) and grants from the National Institutes of Health to S.O.S. (GM 46732 and GM 69651) and S.M. (GM 24971).

* Address correspondence to Steven O. Smith, Department of Biochemistry and Cell Biology, Center for Structural Biology, Stony Brook University, Stony Brook, NY 11794-5215. Tel. 631 632-1210. Fax: 631 632-8575. E-mail: steven.o.smith@sunysb.edu.

‡ Department of Biochemistry and Cell Biology, Center for Structural Biology, Stony Brook University.

§ Department of Physiology and Biophysics, Stony Brook University.

[1] Abbreviations: ATR, attenuated total reflection; CD, circular dichroism; DHPC, 1,2-diheptanoyl-*sn*-glycero-3-phosphocholine; DiD, 1,1′-dioctadecyl-3,3,3′,3′-tetramethylindodicarbocyanine; DMPC, 1,2-dimyristoyl-*sn*-glycero-3-phosphocholine; DMPG, 1,2-dimyristoyl-*sn*-glycero-3-[phospho-*rac*-(1-glycerol)]; EGFR, epidermal growth factor receptor; FRET, fluorescence resonance energy transfer; GUVS, giant unilamellar vesicles; JM, juxtamembrane; LUVS, large unilamellar vesicles; PIP_2, phosphatidylinositol 4,5-bisphosphate; MAS, magic angle spinning; POPC, 1-palmitoyl-2-oleoyl-*sn*-glycero-3-phosphocholine; POPS, 1-palmitoyl-2-oleoyl-*sn*-glycero-3-[phospho-L-serine]; RTK, receptor tyrosine kinase; TM, transmembrane; TOXCAT, ToxR - chloramphenicol acetyltransferase.

10.1021/bi061264m CCC: $33.50
Published on Web 09/30/2006

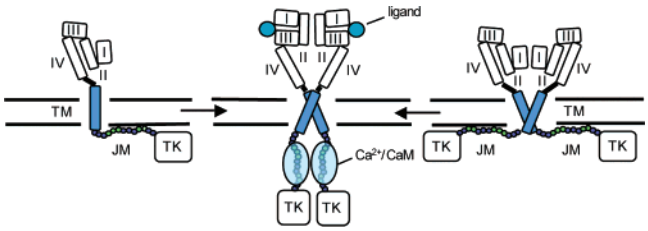

FIGURE 1: Model of the EGFR receptor activation. Ligand binding induces dimerization (left to center pathway) or rearrangement of preformed dimers (right to center pathway). In the extracellular domain of the inactive receptor monomer, there is a direct contact between the cysteine-rich subdomains II and IV. The positively charged JM region and one face of the kinase domain associate with the membrane surface to keep the kinase domains separated. EGF binding triggers rearrangement of the extracellular subdomains in each receptor monomer (*9*, *10*) and releases a dimerization arm on domain II which mediates direct monomer−monomer contacts. Dimerization leads to a well-documented (*3*) rapid increase in the intracellular Ca^{2+} concentration and activation of calmodulin. We propose that binding of the Ca^{2+}/calmodulin complex to the JM region reverses its net charge and allows association of the tyrosine kinase domain (TK in figure). Association of the kinase domains produces allosteric activation by changing the conformation of the activation loop within the kinase domain (*11*).

the release of the kinase domain from the membrane (Figure 1, center). The release of the kinase domain from the membrane would facilitate the formation of a kinase dimer; the allosteric activation mechanism proposed by Zhang et al. (*11*) presumably then produces a change in the conformation of the activation loop and full activation of the kinase. Thus, the electrostatic engine model we previously proposed supplements the mechanism for autoinhibition involving the activation loop.

Key structural features of the model proposed in Figure 1 are a break in the TM helix at the membrane boundary and a flexible JM region that binds electrostatically to the membrane surface. This model contrasts with the idea of rigid rotational coupling of the JM domain with the kinase domain by continuation of the TM α-helix into the cytoplasm (*17*). The studies described here extend our measurements on JM peptides (residues 645−660) to a sequence that includes the full membrane-spanning domain of EGFR reconstituted into bilayer vesicles (*16*). A combination of NMR, CD, infrared, and fluorescence measurements are used to draw three conclusions: (i) the TM helix breaks at the membrane interface; (ii) the unfolded JM region binds electrostatically to the membrane; (iii) binding of Ca^{2+}-calmodulin to the positively charged JM sequence can, under some conditions, reverse its charge and release it from the membrane. These results complement the recent crystal structure studies of the extracellular (*9*, *10*) and kinase (*11*) domains of the EGFR and provide clues to the potential role of the cytoplasmic JM region in receptor activation and regulation.

EXPERIMENTAL PROCEDURES

Materials. Deuterated (5,5,5-d_3) leucine, 1-^{13}C-labeled amino acids and deuterium-free water were purchased from Cambridge Isotope Laboratories (Andover, MA). Other amino acids and octyl-β-glucoside were obtained from Sigma Chemical (St. Louis, MO). DMPC, DMPG, and DHPC were obtained from Avanti Polar Lipids (Alabaster, AL). The tert-butyloxycarbonyl (t-Boc) derivatives of the free amino acids were prepared by James Maracek (Department of Chemistry, Stony Brook University).

Peptide Synthesis and Purification. Peptides corresponding to the TM and JM domains of human EGFR, EGFR(622−660), were synthesized by solid-phase chemistry at the W. M. Keck Facility for Peptide Synthesis at Yale University. Four peptides were synthesized, each containing a single deuterium-labeled leucine at positions Leu631−Leu634 and a single 1-^{13}C-labeled amino acid (Ile640, Leu642, Phe643, Met644, or Ile649). The C-terminus was amidated, and an RRR sequence was added to the N-terminus to increase peptide solubility for synthesis and purification. One of the peptides contained a C-terminal Cys for attaching a fluorescent probe. The numbering of the peptide sequence corresponds to the full length human EGFR:

RRRSIATGMVGALL$_{631}$L$_{632}$L$_{633}$L$_{634}$
VVALGI$_{640}$GL$_{642}$F$_{643}$M$_{644}$RRRHI$_{649}$
VRKRTLRRLLQ-NH$_2$

The synthetic peptides were purified by reverse phase high-pressure liquid chromatography (Varian Prostar) on a C4 column with a 1-propanol-acetonitrile-water gradient (*18*) and lyophilized. The solvents contained 0.1% (w/v) trifluoroacetic acid. The purity was confirmed with MALDI mass spectrometry and high-pressure liquid chromatography.

Preparation of Isotropic Bicelles. DMPC−DMPG−DHPC bicelles, consisting of 10% (w/v) phospholipids, were prepared in a 30 mL vial. The final molar ratio (q) of long-chain DMPC and DMPG to short-chain DHPC was 1.0. DMPC and DMPG, in the molar ratio of 10:3, were first dissolved in a mixture of cyclohexane and ethanol, and the resultant solution was lyophilized to give a homogeneously mixed powder of DMPC and DMPG. DHPC was separately dissolved in a mixture of chloroform, and the solvent was removed under reduced pressure. The dried film of DHPC was rehydrated with 20 mM sodium phosphate buffer (pH 7.0). The solution was subjected to several freeze and thaw cycles, and the resultant DHPC solution was used to rehydrate the powder mixture of DMPC and DMPG to yield a final molar ratio of DMPC, DMPG, and DHPC of 10:3:13. The mixture of three phospholipids in buffer was incubated at 37 °C for 15 min and then at 4 °C for 30 min. This temperature cycle was repeated until a clear solution was obtained.

Reconstitution of EGFR(622−660) into Vesicles. Peptides were reconstituted into DMPC−DMPG vesicles at a peptide to lipid molar ratio of 1:50 by detergent dialysis (*19*). In contrast to the binding of the hydrophilic JM domain peptides to bicelles, the reconstitution of hydrophobic TM domain peptides requires detergent dialysis to prevent nonspecific peptide aggregation (*19*). The molar ratio of DMPC to DMPG was 10:3. Lipid, peptide, and detergent (*n*-octyl-β-glucoside) were co-solubilized in a mixture of trifluoroethanol and chloroform and incubated at 37 °C for over 2 h. The organic solvents were removed by evaporation using a stream of argon gas, and the resultant film was dried under reduced pressure. The dry mixture was rehydrated with phosphate buffer (5 mM phosphate, 50 mM sodium chloride, 5 mM dithiothreitol, pH 6.0) such that the final concentration of *n*-octyl-β-glucoside was 5% (w/v). The rehydrated sample was then stirred slowly for at least 6 h. Dialysis was

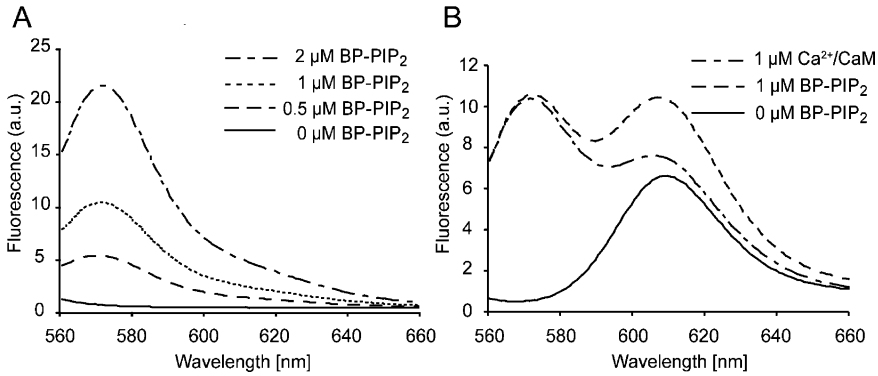

FIGURE 2: (A) Incorporation of Bodipy-TMR-PIP_2 into large unilamellar vesicles composed of POPC produces a linear increase in Bodipy-TMR fluorescence intensity. Each curve in the graph corresponds to the emission spectrum of Bodipy-TMR incorporated into POPC LUVs (total lipid concentration 500 μM). (B) Ca^{2+}/calmodulin disrupts FRET between Bodipy-TMR-PIP_2 and Texas Red EGFR(622−660). The curves represent raw uncorrected data. The lower curve represents the emission spectrum from vesicles (lipid concentration at start of reconstitution = 500 μM) containing reconstituted EGFR(622−660) labeled with Texas Red. The upper curve represents the spectrum of the same vesicles after incorporation of 1 μM Bodipy-TMR-PIP_2. The increase in the fluorescence intensity at ~570 is due to Bodipy-TMR, as shown in panel A. The increase in fluorescence intensity at ~610 is due to FRET. The middle curve represents the spectrum of the same vesicles after addition of 1 μM Ca^{2+}/calmodulin. Note the decrease in FRET. Addition of Ca^{2+} alone or calmodulin with EGTA does not decrease FRET (not shown). The solutions contain: [KCl] = 100 mM; [MOPS] = 10 mM; [EGTA] = 0.2 mM; pH 7.

performed to remove the *n*-octyl-β-glucoside using Spectra-Por dialysis tubing (3500 MW cutoff) for 48 h against phosphate buffer at 37 °C. The bilayers were then pelleted, resuspended in deuterium-depleted water, and incubated at 37 °C for more than 24 h. The reconstituted vesicles were pelleted and loaded into NMR rotors.

Polarized IR Spectroscopy. Polarized attenuated total reflection (ATR) FTIR spectra were obtained on a Bruker IFS 66V/S spectrometer. Membrane vesicles at a concentration of 10 mg lipid/mL were layered on a germanium internal reflection element using a slow flow of air directed at an oblique angle to the ATR plate to form an oriented multilamellar lipid-peptide film. Each sample spectrum represents the average of 1000 scans acquired at a resolution of 4 cm^{-1}.

The dichroic ratio (R^{ATR}) is defined as the ratio between absorption of parallel ($A_{||}$) and perpendicular ($A_{\perp}$) polarized light (*19*). The observed dichroic ratio is used to calculate the order parameter S_{meas} using the equation

$$S_{meas} = \frac{E_x^2 - R^{ATR} E_y^2 + E_z^2}{E_x^2 - R^{ATR} E_y^2 - 2E_z^2} = \frac{3\cos^2\theta - 1}{2}\left[\frac{3\cos^2\alpha - 1}{2}\right]S_{mem}$$

Order parameters (S_{meas}) of 1.0 and −0.5 correspond to helical orientations parallel and perpendicular to the membrane normal, respectively. The order parameter depends on the electric field amplitudes in the thick film limit which is applicable for our experiments, namely, $E_x = 1.399$, $E_y = 1.514$, and $E_z = 1.621$. θ is the angle between the helix director and the normal of the internal-reflection element, and *a* is the angle between the helix director and the transition-dipole moment of the amide I vibrational mode. To calculate the angle θ between the helix director and the normal of the ATR plate, one must know the value of the transition moment angle α. We use a value of 39.5° based on parallel measurements on bacteriorhodopsin as previously discussed (*20*) and assume that the minimum disorder in the sample corresponds to an order parameter S_{mem} of 0.85.

Circular Dichroism Spectroscopy. CD spectra were obtained on an Olis Instruments spectrophotometer using isotropic bicelles and a path length of 0.2 mm. The ratio of DMPC/DMPG/DHPC was 10:3:13, and the total lipid concentration was 10% by volume in 20 mM sodium phosphate buffer (500 μL) at pH 7.0. The peptide (0.15 mg, 8.8×10^8 mol) was added after the bicelles were formed to yield a peptide to lipid molar ratio of 1:100.

Fluorescence Resonance Energy Transfer (FRET). FRET experiments were performed on an SML AMINCO spectrofluorometer. We measured the energy transfer between a Bodipy-TMR label on PIP_2 and a Texas-Red label attached to a C-terminal cysteine of EGFR(622−660) as described previously (*21*). Bodipy-TMR was the donor, and Texas-Red was the acceptor fluorophore. We excited at the donor excitation wavelength of 547 nm and collected emission spectra from 560 to 660 nm. EGFR(622−660) was reconstituted as above (i.e., through detergent dialysis) into membrane vesicles composed of either POPC, or POPC and POPS at a molar ratio of 5:1. Bodipy-TMR-PIP_2 was incorporated into the vesicles by the addition of Bodipy-TMR-PIP_2 micelles to the vesicle solution.

We first performed control experiments showing that incorporation of Bodipy-TMR-PIP_2 into large unilamellar vesicles (LUVs) composed of POPC [without EGFR(622−660) peptide] produces a linear increase in the Bodipy-TMR fluorescence in the concentration range used in our experiments (Figure 2A). We collected emission spectra from POPC LUVs (total lipid concentration 500 μM) with 0, 0.5, 1, and 2 μM Bodipy-TMR-PIP_2 incorporated from micelles (*22*).

We next monitored FRET as an increasing amount of Bodipy-TMR-PIP_2 was incorporated into the POPC vesicles reconstituted with EGFR(622−660) peptide. Figure 2B shows an example of the raw data we collected. To correct the data and produce the curves shown in Results (Figure 7), we subtracted both the scaled signal of Bodipy-TMR fluorescence from Figure 2A and the signal from Texas-Red taken when no Bodipy-TMR-PIP_2 was present in the vesicles (e.g., the 0 μM BP-PIP_2 curve in Figure 2B).

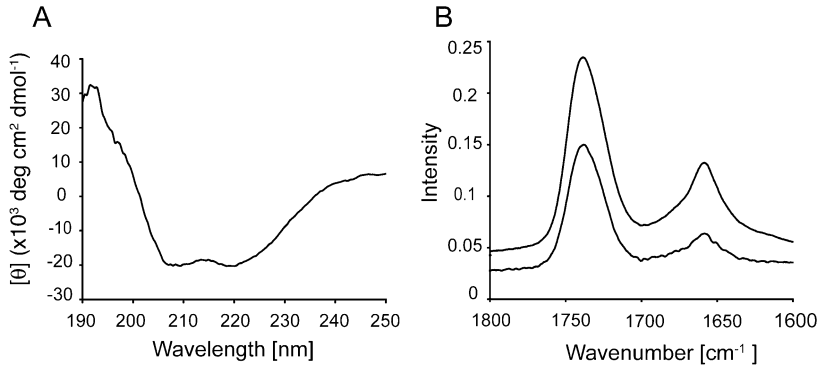

FIGURE 3: Secondary structure of EGFR(622−660). (A) CD spectra of EGFR(622−660) reconstituted into isotropic ($q = 1$) bicelles exhibit minima at 208 and 220 nm, and a maximum at 193 nm characteristic of α-helical secondary structure. (B) Polarized ATR IR spectra of EGFR(622−660) reconstituted in multilamellar vesicles obtained with parallel (top curve) and perpendicular (bottom curve) polarized light. The narrow amide I vibration observed at 1655 cm^{-1} is characteristic of α-helical secondary structure. The high dichroic ratio of the amide I band is consistent with a transmembrane orientation for the helix.

Solid-State NMR Spectroscopy. Solid-state NMR magic angle spinning (MAS) experiments were performed at 55 MHz (^{2}H observe) or 90.2 MHz (^{13}C observe) on a Bruker Avance NMR spectrometer using a 4.0 mm MAS probe. For ^{13}C observe MAS experiments, the MAS frequency was maintained at 8 kHz ± 5 Hz. Ramped amplitude cross polarization (*23*) contact times were 2 ms and two-pulse phase-modulated decoupling (*24*) was used during the evolution and acquisition periods. The decoupling field strength was typically 90 kHz. ^{13}C chemical shifts were referenced to external tetramethylsilane. The temperature was maintained at −75 °C.

For the ^{2}H observe experiments, the MAS frequency was maintained at 3 kHz ± 5 Hz to have a sufficient number of spinning side bands to define the static line shape. Single pulse excitation was employed with a 3.7 μs 90° pulse length, followed by a 4.5 μs delay before data acquisition. The repetition delay was 250 ms. A total of 600,000−800,000 transients were averaged for each spectrum and processed using a 200 Hz exponential line broadening function. Spectra were obtained at 25 °C.

MAS deuterium spectra were simulated using the program SIMPSON version 1.1.0 (*25*) with a spin rate of 3.0 kHz. The asymmetry parameter (η) was set to 1.0. Only the quadrupole coupling constant was varied to quantify the width of the envelope traced out by the MAS side bands.

RESULTS

EGFR(622−660) Spans Model Membranes with α-Helical Secondary Structure. The extracellular, TM, and cytoplasmic sequences of the EGFR independently fold into distinct domains. The crystal structures of the extracellular (*9*, *10*) and kinase (*11*) domains have been determined to high resolution. However, much less is known about the structure of the TM domain or of the JM region that links the TM to the kinase domain. The TM and associated JM sequences require a membrane environment for structural studies. Here, we use either membrane bilayers or bicelles to characterize the structure of the TM and JM regions of EGFR in the context of a lipid bilayer environment. In studies of TM peptides (with no intrinsic activity), it is important to show that the reconstitution procedure yields a peptide that spans the bilayer in a helical orientation. Hydrophobic peptides have a strong tendency to nonspecifically aggregate during membrane reconstitution. After establishing that the peptide is reconstituted in a helical TM orientation, we address the structure of the JM domain. We consider only the N-terminal portion (residues 645−660) of the JM region, which has previously been shown to bind Ca^{2+}/calmodulin as an isolated 16-residue peptide (*16*). The C-terminal portion (673−682) of the JM region is associated with the kinase domain (*26*), while the middle portion (661−672), which has a net negative charge, may act as a flexible linker due to two central prolines.

Figure 3 presents the CD and polarized FTIR spectra of EGFR(622−660). CD spectra were obtained of EGFR(622−660) reconstituted into membrane bicelles. The ratio (or q value) of long-chain (DMPC and DMPG) to short-chain (DHPC) lipids determines the morphology of the bicelle (*27*). Isotropic bicelles with a 1:1 ratio of long- to short-chain lipids ($q = 1$) are used, rather than multilamellar vesicles, to lower the level of light scattering that results in attenuation and a red shift of the observed CD bands. The CD spectrum of EGFR(622−660) in Figure 3A exhibits distinct minima at 208 and 220 nm, and a maximum at 193 nm. These features are characteristic of α-helical secondary structure. The amount of helical structure can be estimated from the magnitude of the minima at 208 and 220 nm. On the basis of soluble protein data sets, helical secondary structure exhibits minima at 208 and 220 nm with molar ellipticities of approximately −36 000 ± 3000 deg cm^2 $dmol^{-1}$ (*28*). The observed molar ellipticity of −21 000 deg cm^2 $dmol^{-1}$ indicates that ∼60% of the EGFR(622−660) peptide is helical. The observed helical structure likely corresponds to the ∼25 membrane-spanning amino acids of EGFR(622−660) (see below).

Figure 3B presents polarized IR spectra of EGFR(622−660) reconstituted into multilamellar vesicles and layered onto a germanium IR plate. The spectra obtained with light having parallel and perpendicular polarization exhibit an amide I vibration at 1655 cm^{-1} characteristic of α-helical secondary structure (*29*). The amide I band is relatively narrow, although there is a broad component that we attribute to the unstructured JM region. The dichroic ratio of the amide I band (before Fourier deconvolution) is 3.2, corresponding to a maximum helix tilt relative to the bilayer normal of ∼23°. Fourier deconvolution does not resolve the helical and unstructured components since both are centered at ∼1655

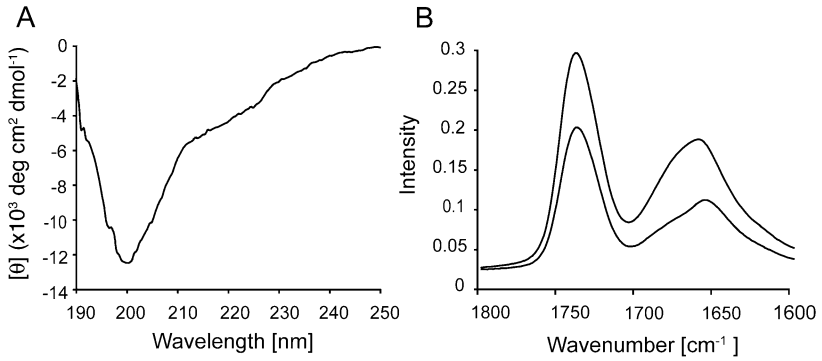

FIGURE 4: Secondary structure of EGFR(645−660). (A) CD spectra of EGFR(645−660) obtained by titrating EGFR(645−660) into a solution of isotropic bicelles exhibit a minimium at ∼200 nm, indicative of random coil. (B) Polarized ATR IR spectra of EGFR (645−660) associated with DMPC/DMPG multilamellar vesicles obtained with parallel (top curve) and perpendicular (bottom curve) polarized light. The broad amide I vibration is observed at 1660 cm^{-1} with a distinct shoulder at 1680 cm^{-1}, consistent with random coil. The negative membrane surface charge due to the DMPG incorporated into the bicelles in (A) or the vesicles in (B) results in binding of the positively charged EGFR(645−660) peptide (*16*).

cm^{-1}. There is clearly no β-strand structure in the reconstituted peptide, which would exhibit a frequency of ∼1630 cm^{-1} if present. If one accounts for the unstructured JM domain of the EGFR(622−660) peptide, then the dichroic ratio of the TM region alone is greater than 3.2 and the TM helix axis is closer to the bilayer normal.

The EGFR(622−660) Transmembrane Helix Breaks at the Cytoplasmic Membrane Surface. On the basis of the CD and polarized IR spectra in Figure 3, we can conclude, at a minimum, that the TM region of the EGFR(622−660) peptide spans the membrane bilayer in a helical conformation after reconstitution. The next question we address is whether the secondary structure of the JM domain is helical or random coil. There was no evidence of β-strand structure in the full TM-JM peptide by polarized IR spectroscopy; rather, the analysis of the IR spectra suggested that the JM region is random coil. Parallel CD spectra of the JM region alone, EGFR(645−660), reveal a strong negative signal at 200 nm characteristic of random coil (Figure 4A). In addition, polarized IR spectra of membrane-bound EGFR(645−660) in Figure 4B exhibit a broadband centered at ∼1660 cm^{-1} with a dichroic ratio of 1.8. These features are characteristic of random coil (*29*).

To address where the TM helix breaks and forms random coil or extended secondary structure, we obtained ^{13}C spectra of the TM−JM peptide, EGFR(622−660), containing specific backbone ^{13}C labels at the putative TM−JM boundary. The TM−JM peptide was reconstituted into DMPC/DMPG lipid vesicles for these experiments. The carbonyl carbon ^{13}C chemical shifts are sensitive to secondary structure (*30*). Saito and Naito (*31*) have correlated chemical shifts from solid-state NMR studies of fibrous and membrane proteins and have found that in helical secondary structure, carbonyl carbons exhibit chemical shifts in the range of 173−176 ppm, while in random coil and β-strand structure they are in the range of 168−172 ppm (*31*). An analysis of the chemical shifts in the TALOS database of soluble proteins (http://spin.niddk.nih.gov/NMRPipe/talos/) shows that the carbonyl chemical shifts of the amino acids studied here (Ile, Leu, Met, and Phe) are centered at ∼178 ppm for α-helix and ∼175 ppm for β-sheet, with a standard deviation of ∼1.5 ppm. This means that the measurement of a single ^{13}C═O chemical shift is not sufficient to define the secondary structure at a specific site. However, a characteristic difference of ∼3 ppm for a transition from α-helical to random coil or β-strand secondary structure within a peptide sequence suggests a simple way to probe where TM helix breaks in the EGFR(622−660) peptide.

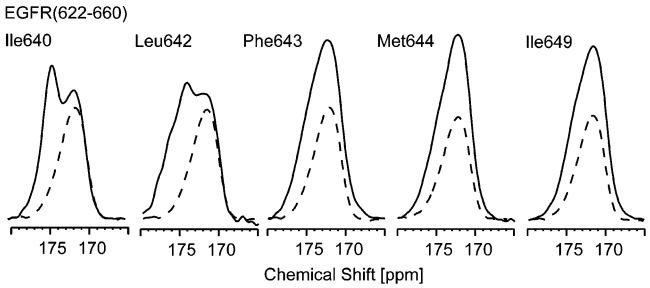

FIGURE 5: ^{13}C MAS NMR of EGFR(622−660). EGFR (622−660) peptides contain a single ^{13}C═O labeled amino acid at Ile640, Leu642, Phe643, Met644, or Ile649. The spectra were obtained at a spinning frequency of 8 kHz and a temperature of −75 °C.

Figure 5 presents MAS NMR spectra of EGFR(622−660) specifically ^{13}C-labeled at the backbone carbonyl in the TM and JM regions of the peptide. MAS spectra of DMPC and DMPG multilayers were obtained with (solid line) and without (dashed line) reconstituted EGFR(622−660) peptide. Only the ^{13}C═O region of the MAS spectrum is shown. Without peptide, only the natural abundance ^{13}C carbons of the lipid acyl chain carbonyls at ∼172 ppm are observed (dashed line). The spectra of EGFR(622−660) containing 1-^{13}C Ile640 and 1-^{13}C Leu642 exhibit two resonances. The resonance at ∼175 ppm is assigned to the specific backbone ^{13}C═O, and the resonance at ∼172 ppm is assigned to the lipid acyl chain carbonyls. In contrast, the 1-^{13}C resonances of the next two amino acids in the EGFR(622−660) sequence, Phe643 and Met644, are centered at ∼172 ppm co-incident with the chemical shift of the natural abundance ^{13}C of the lipid acyl chain carbonyls. A similar shift is observed for Ile649 which is well into the JM region of EGFR(622−660). On the basis of these ^{13}C═O chemical shifts, the intrahelical hydrogen bond between Leu642 and Arg646 marks the last turn of the TM helix. The sequence beyond Arg646 is non-helical. A similar conclusion was reached by Rigby et al. (*32*) on the basis of solution NMR studies of EGFR(621−654) in TFE and TFE−water mixtures. They observed α-helical secondary structure up to Arg647.

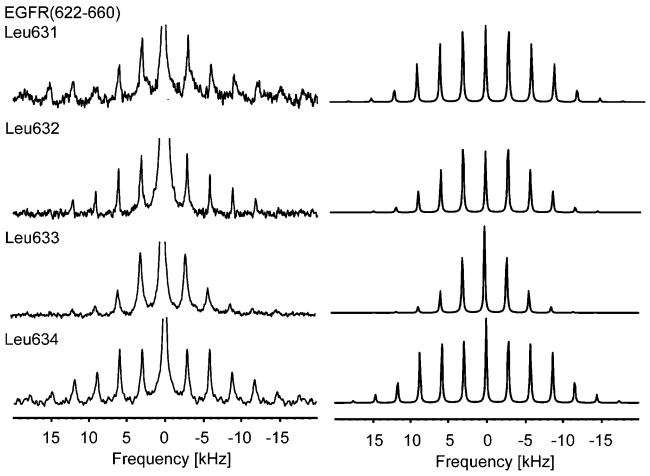

FIGURE 6: Deuterium MAS NMR of EGFR (622−660). EGFR (622−660) peptides contain a single deuterated leucine at Leu631, Leu632, Leu633, or Leu634. The MAS spectra were obtained at a spinning frequency of 3 kHz and a temperature of 25 °C. The simulations to the right were carried out using the program SIMPSON version 1.1.0 (*25*). The MAS rate was set to 3 kHz and the asymmetry parameter was set to 1.0. The best fits to the observed sideband intensities were obtained using quadrupole coupling constants of 16 kHz (Leu631), 14 kHz (Leu632), 10 kHz (Leu633), and 19 kHz (Leu634).

Association of EGFR(622−660) Transmembrane Helices in Model Membranes. Deuterium NMR spectroscopy in combination with MAS is used to determine if the TM regions of the EGFR(622−660) peptides associate in membrane bilayers and whether there is a preferential face for association. Deuterium NMR spectroscopy takes advantage of the sensitivity of deuterium lineshapes to molecular motion (*33*−*35*). MAS enhances the sensitivity. We have previously shown that the motion of amino acids located in TM helix−helix interfaces is restricted relative to amino acids oriented toward the lipid membrane (*20*). Leucine containing a single deuterated methyl group at the end of its long flexible side chain is a particularly sensitive probe for restriction of motion. By characterizing side chain motion as a function of the TM sequence, one can map out the interface of interacting TM helices.

The approach taken here is to compare spectra of EGFR-(622−660) containing deuterated (5,5,5-d_3) leucine at different positions in the sequence. We compare the deuterium spectra of four consecutive leucines in the TM sequence: Leu631, Leu632, Leu633, and Leu634. The polarized IR spectra above show that the TM region of EGFR(622−660) is helical, and consequently these four residues constitute one full turn of the EGFR(622−660) α-helix. If the TM sequence dimerizes, at least one of the leucine side chains will be facing the helix dimer interface and will exhibit a broader deuterium spectrum due to restricted motion.

Figure 6 presents deuterium MAS NMR spectra of the four EGFR(622−660) peptides containing a single deuterated leucine. MAS is used to increase sensitivity. The intensities of the side bands in the MAS deuterium spectra trace out the broad deuterium lineshapes. The first revealing aspect of the spectra in Figure 6 is that there is significant intensity in the MAS sidebands. Monomeric reconstituted TM peptides containing deuterated leucine exhibit intensity mainly in the central isotropic resonance, presumably due to faster axial rotation of the peptide (unpublished data).

Comparison of the spectra shows that the intensity distribution in the side bands differs between the four sites. Leu634 exhibits the broadest sideband envelope, while Leu633 exhibits the narrowest envelope. To roughly quantify the observed differences in the width of these lineshapes, we simulated the MAS deuterium spectra using the quadrupole coupling constant as the only free parameter. The simulations assume that the lineshapes have an asymmetry parameter (η) of 1 due to high motional averaging. This assumption is based on experimental and theoretical studies by Torchia and co-workers (*36*) who modeled the static lineshapes of deuterated leucine in amino acid model compounds and in collagen. They found that the leucine methyl deuterons in collagen exhibit axially symmetric lineshapes ($\eta = 0$) at low temperature (−85 °C), but yield lineshapes with an asymmetry parameter of nearly 1 above ∼ +15 °C (*36*). Axially symmetric lineshapes with a quadrupolar splitting of ∼40 kHz are characteristic of methyl groups undergoing fast three site hops, while the narrower lineshapes with an η of ∼1 are due to *additional* averaging by rotation or two site hopes about the Cα−Cβ bond of the leucine side chain. We used this approach previously to simulate the side band intensities of leucine residues around one turn of a helix in the TM dimer of gp55-P (*20*).

The quadrupole coupling constant (QCC) needed to best fit the spectrum of Leu634 (19 kHz) is nearly twice the size of the QCC needed to best fit the spectrum of Leu633 (10 kHz). (The differences in the values of the QCC needed to fit the lineshapes reflect the effects of motional averaging; the actual quadrupole coupling constants of the C−D bonds do not change.) For comparison, in the dimer structure of gp55-P previously analyzed by this approach (*20*), the interfacial leucine was best fit with a QCC of 25 kHz, while the lipid facing leucine exhibited a QCC of 14 kHz. The spectrum of Leu631 is not fit well by this approach since it exhibits both a broad component and a narrow component, possibly due to two different leucine conformations. In this case, the QCC of only the broad component of the spectrum was estimated by eliminating the first MAS sideband in the analysis. Nevertheless, this comparison supports the conclusion that the EGFR peptides associate in membranes and suggests that they associate in an orientation that favors the helical face containing Leu634.

Grant and co-workers have also characterized the association of EGFR TM peptides using deuterium NMR (*32*, *37*−*39*). In their studies, they obtained spectra of the EGFR(621−654) containing deuterated alanine, methionine and valine. The spectra were obtained without MAS using peptide:lipid molar ratios between 1:17 and 1:100. Their results are consistent with the studies here; they show that the EGFR TM domain associates in membranes and that the face containing Ala637 in the wild-type sequence preferentially associates over the face containing Ala629. Ala637 is roughly on the same helical face as Leu634. It is important to note that in both our studies and those of Grant and co-workers, the peptide/lipid molar ratios are relatively high (≥1:100). While this is considerably higher than the ratios found in cell membranes, the observed helix−helix interactions may well be important when EGF mediates dimer formation and brings the TM domains into close proximity.

Reversible Binding of the JM Sequence of EGFR(622−660). The NMR and polarized IR measurements of EGFR-

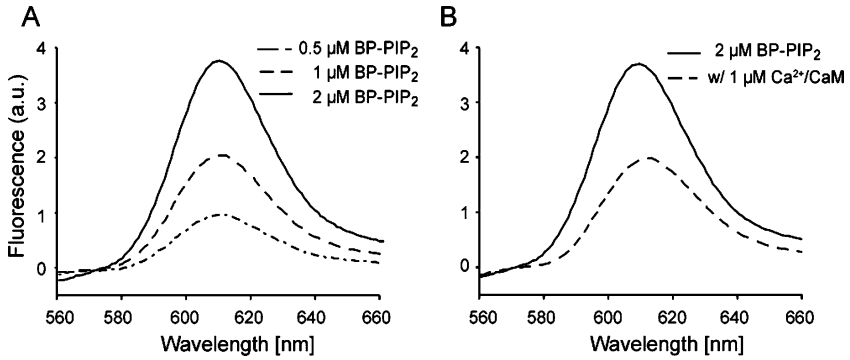

FIGURE 7: Reversible binding of the JM sequence of EGFR(622−660) to the surface of membrane bilayers. The fluorescence emission spectra are shown for a Texas-Red fluorescent probe (emission wavelength ~ 610 nm) attached to the C-terminal cysteine of the EGFR-(622−660) TM−JM peptide reconstituted into membrane vesicles. (A) Corrected spectra showing FRET from the Bodipy-TMR label on PIP_2 to the Texas-Red label on EGFR(622−660) as a function of Bodipy-TMR-PIP_2 (BP-PIP_2) concentration. FRET increases as the Bodipy-TMR-PIP_2 concentration is increased from 0 to 0.5, 1, and 2 μM. (B) Corrected spectra showing FRET from Bodipy-TMR-PIP_2 to the Texas-Red-EGFR(622−660) decreases upon addition of Ca^{2+}/calmodulin. FRET increases with the addition of 2 μM Bodipy-TMR-PIP_2 as shown above. Addition of either 240 μM Ca^{2+} or calmodulin + EGTA does not appreciably change the fluorescence emission. However, the addition of 1 μM Ca^{2+}/calmodulin partially reverses the FRET observed with the addition of Bodipy-TMR-PIP_2

(622−660) are consistent with the structure for the TM and JM regions shown in Figure 1. The TM sequence spans the cell membrane in helical secondary structure that breaks at the cytoplasmic membrane surface. In this section, we address three questions: does the JM region bind to the membrane, does it sequester PIP_2, and is Ca^{2+}/calmodulin able to pull the JM region from the membrane surface in the context of the full TM−JM sequence? We have previously shown that Ca^{2+}/calmodulin has a high affinity ($K_d \approx$ 10 nM) for a peptide corresponding to the JM region alone (residues 645−660) and is able to extract peptides corresponding to JM sequence from the surface of negatively charged membrane vesicles (*16*).

Binding of the JM sequence to the membrane was measured using FRET between a fluorescent Bodipy-TMR label on PIP_2 and a Texas-Red label attached to a C-terminal cysteine of the TM-JM peptide, EGFR(622−660) (*16*). Bodipy-TMR is the donor and Texas-Red is the acceptor in these experiments. Bodipy-TMR is excited using 547 nm light, and fluorescence emission from Texas-Red is monitored in the region from 560 to 660 nm. The Bodipy-TMR PIP_2 can be incorporated into POPC and POPC/POPS vesicles by adding a solution of fluorescent PIP_2 micelles to the preformed vesicles (*22*). The micelles allow the fluorescent PIP_2 to partition into the outer leaflet of the vesicles. [The partitioning of the PIP_2 monomers is manifested as a 10-fold increase in fluorescence upon incorporation due to lack of self-quenching. As shown in the methods section, the fluorescence of PC vesicles increases linearly with the mole fraction of PIP_2 incorporated under our conditions. Furthermore, measurements using fluorescence correlation spectroscopy on giant unilamellar vesicles (GUVS) show PIP_2 incorporated using this micelle approach has the expected diffusion constant of 3×10^{-8} cm^2/s characteristic of other lipids in these GUVS (*22*). These data provide support that the PIP_2 from the micelles is actually incorporating as monomers into the vesicles containing the reconstituted TM-JM peptides.] Use of the highly negatively charged PIP_2 adds an important biological component to these experiments since binding of the positively charged JM sequence to the membrane surface produces a local positive electrostatic potential that may laterally sequester PIP_2 (*40*). PIP_2 is a substrate of two enzymes bound to activated EGFR and interacts with a number of other modular membrane targeting domains (*41*). The shorter JM peptide, EGFR(645−660), is able to laterally sequester PIP_2 when it binds to a PC/PS/PIP_2 membrane (*16*).

Figure 7A presents the results of a typical FRET experiment where the Texas-Red labeled EGFR(622−660) peptide was reconstituted into POPC membrane vesicles using a detergent dialysis approach and the PIP_2 concentration was increased from 0 to 0.5, 1 and 2 μM immediately before the fluorescence experiment. The FRET increases linearly with the PIP_2 incorporated into the vesicle. The raw data (see Experimental Procedures) show some fluorescence emission from Bodipy-TMR-PIP_2 at 571 nm, but the significant feature is the enhanced fluorescence emission (i.e., FRET) from Texas-Red observed at 607 nm. The data in Figure 7A is corrected for the fluorescence of both PIP_2 and the initial fluorescence level of Texas Red. The simplest interpretation of the observed FRET from Bodipy-TMR-PIP_2 to Texas-Red is that the Texas-Red label at the C-terminus of the peptide, and thus the JM region of the EGFR(622−660) peptide, is bound to the membrane. A similar conclusion was reached using two different approaches (data not shown): an acrylodan label at the C-terminus of EGFR(622−660) is quenched by NBD-labeled PS in the membrane and the Texas-Red label on EGFR(622−660) is quenched by 1,1′-dioctadecyl-3,3,3′,3′-tetramethylindodicarbocyanine (DiD).

Figure 7B shows the influence of Ca^{2+}/calmodulin on FRET (corrected spectra). First, the addition of 2 μM PIP_2 to POPC membrane vesicles containing EGFR(622−660) results in FRET and an increase in fluorescence at 607 nm, as observed in Figure 7A. The subsequent addition of 240 μM Ca^{2+} (or 1 μM calmodulin without Ca^{2+}) has only a moderate effect on the fluorescence emission (data not shown). However, the addition of 1 μM Ca^{2+}/calmodulin reverses about 50% of the FRET observed with the addition of PIP_2. If only 1000 or 500 nM PIP_2 was used, and the affinity of the JM region for the membrane is thus weaker, Ca^{2+} /calmodulin produced a larger % reversal in the FRET (data not shown). The simplest interpretation of the decrease in FRET is that Ca^{2+}/calmodulin can bind to the JM region and release it from the membrane. More striking effects can also be observed when the fluorescence from the Texas-Red label is quenched with DiD (or from acrylodan quenched

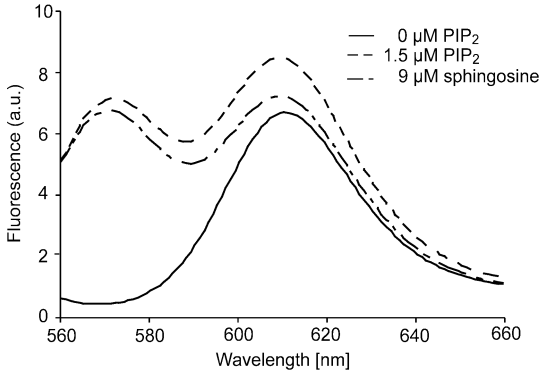

FIGURE 8: FRET between Bodipy-TMR-PIP_2 and Texas-Red-EGFR(622−660) decreases with the addition of the amphipathic weak base sphingosine. The lower curve represents the signal from 5:1 PC/PS vesicles containing Texas-Red labeled EGFR(622−660). The addition of 1.5 μM Bodipy-TMR-PIP_2 produces an enhanced signal at ∼610 nm, i.e., FRET (upper curve). The addition of 9 μM sphingosine produces a significant decrease in the FRET. It is important to note that the final lipid concentration in these experiments was ∼50 μM due to loss of sample in the reconstitution process. As a result, the 9 μM sphingosine required to cause the JM region to desorb from the PC/PS membranes is presumably because the PS concentration is ∼10 μM (i.e., ∼10 μM sphingosine is needed to reverse the negative charge from PS).

with NBD-PS). In these experiments, the TM−JM peptide was reconstituted into 20:1 PC/PS vesicles. Adding 1 mM Ca^{2+}/calmodulin produces a large increase in the fluorescence (∼2 fold), again suggesting that the JM region of the TM−JM peptide is bound to the membrane, and the binding can be released by Ca^{2+}/calmodulin (data not shown).

As a control, Figure 8 shows the influence of sphingosine on FRET. Sphingosine is an amphipathic weak base that binds to membranes, and electrophoretic mobility measurements show it will reverse the charge of the PC/PS membrane in the concentration range used (*16*). As a result, sphingosine should electrostatically repel the positively charged JM region of the TM−JM peptide from the membrane. In these experiments, 1.5 μM PIP_2 was added to membrane vesicles composed of POPC and POPS in a 5:1 molar ratio and reconstituted with EGFR(622−660). The addition of PIP_2 produces FRET between the Bodipy label on PIP_2 and the Texas-Red label on the C-terminus of EGFR(622−660). The strong observed FRET indicates that PIP_2 can be laterally sequestered, even when PS is present in excess. These results are consistent with those found with the JM peptide alone (*16*). The lateral sequestration of PIP_2 by basic membrane-bound clusters is expected from electrostatic calculations (*40*). However, we found that 1 μM Ca^{2+}/calmodulin will not pull the JM region of the TM−JM peptide off the membrane when reconstituted into the 5:1 PC/PS vesicles.

Importantly, the fluorescence emission at 607 nm is reversed to the initial value by the addition of 9 μM sphingosine consistent with the release of the JM region of the EGFR(622−660) peptide from the membrane surface. (Lower sphingosine concentrations, have intermediate effects, as expected.) These concentrations of sphingosine (1−10 μM) also release the JM peptide EGFR(645−660) from the membrane (*16*). Of note is that the addition of 2 μM sphingosine to intact cells and broken cell membranes activates (i.e., produces intermolecular autophosphorylation) EGFR in the absence of EGF (*42*), as predicted by our model for EGFR activation in Figure 1 (*16*).

DISCUSSION

There are several clues that the TM−JM region of the EGFR is not merely a passive element in the receptor structure and that its role in receptor activation and regulation is likely to be unique among the receptor tyrosine kinases. For example, phosphorylation of Thr654 within the cytoplasmic JM sequence by protein kinase C inhibits receptor activity (*43*, *44*). In contrast, phosphorylation of JM tyrosines in other RTKs, such as the EphB2 (*45*) and FLT3 receptors (*46*), helps relieve autoinhibition. In these receptors, the cytoplasmic JM region binds to the kinase domain and can prevent the activation loop from adopting an active conformation. In the EGFR, however, only tyrosines in the C-terminal tail are normally phosphorylated.

The X-ray crystal structure of the kinase domain plus a portion of the JM region (*26*) and the solution NMR structure of the JM region plus a portion of the kinase domain (*47*, *48*) suggest the N-terminal JM sequence of the EGFR is likely to be flexible, rather than forming a rigid connection between the TM and the kinase domains. The first resolved residue in the EGFR crystal structure of the kinase domain (plus a portion of the JM domain) is Gly672. The six amino acids preceding Gly672 are not resolved (suggesting flexibility of this region of the JM domain), while the succeeding 13 amino acids (the C-terminal portion of the JM domain) have an extended structure that is tied by hydrophobic and hydrogen-bonding interactions to the well-defined β-sheet of the N-terminal lobe of the kinase domain (*26*).

In contrast to the X-ray structure, the solution NMR structure of the JM sequence plus ∼12 residues of the N-terminal lobe of the kinase domain (residues Arg645-Gly697) reveals three amphipathic, helical segments when bound to dodecylphosphocholine micelles. In agreement with the crystal structure, the region just before Gly672 (i.e., Glu661−Gly672), which is negatively charged and contains a central PxxP sequence, is unstructured (*48*). Our results appear to disagree with the solution NMR studies: the N-terminal JM helix (residues 652−661) observed in their studies overlaps the unstructured JM sequence in our TM−JM peptides. However, Sonnichsen and co-workers (*48*) point out that this helix may be nucleated by interactions with the C-terminal helices since it was not observed in NMR measurements of a 30-residue JM peptide (Arg645−Ala674) (*47*). For the experiments described above, we only include the N-terminal portion of the JM sequence that contains positively charged and hydrophobic amino acids and ends at the first residue (Glu661) of the "flexible linker". As noted above, short peptides corresponding to this N-terminal JM sequence are unstructured when bound to membrane surfaces and are able to bind Ca^{2+}/calmodulin with high affinity (*16*). With our TM−JM construct, we can address the structure and membrane interactions of the N-terminal JM region in the context of the TM domain. The major conclusions of our studies are that (i) the helical TM domain breaks at the TM−JM boundary, (ii) the JM region associates with the membrane surface with the ability to sequester PIP_2, and (iii) Ca^{2+}/calmodulin can pull the JM region from the membrane surface.

The Positively Charged JM Domain of EGFR Binds to Membranes and Interacts with Ca^{2+}/Calmodulin. Ullrich et al. (*49*) and Hunter et al. (*43*) first suggested that the

positively charged JM region should bind to membranes and be in a position to modulate signaling between the ligand-binding domain and kinase domain. We provided experimental evidence that a peptide corresponding to the JM domain is unstructured and binds strongly to membranes (*16*). As with other basic peptides, binding increases exponentially with the mole fraction of acidic lipid. These studies, however, have left open the question of whether the JM region would bind in context of TM−JM sequence. Results here show it does, even when the bilayer contains as little as 1% PIP_2 or 5% PS. Furthermore, when bound the JM region can laterally sequester PIP_2.

The fluorescence experiments using Bodipy-TMR-PIP_2 and Texas-Red EGFR(622−660) show that the JM region is able to sequester PIP_2 through nonspecific electrostatic interactions. PIP_2 is the most abundant of the poly-phosphoinositides and comprises about 1% of the total phospholipids in plasma membranes (*50*−*52*). Hydrolysis of PIP_2 by phospholipase Cs forms diacylglycerol and inositol 1,4,5-trisphosphate, two important second messengers involved in signal transduction within cells. Phosphorylation of PIP_2 by PI_3-kinase forms PIP_3, another important signaling molecule. PLC-γ and PI-3K are bound to the C-terminal tail of activated (autophosphorylated) ErbB family receptors, which suggests the reversible sequestration of their substrate by the JM region may be of biological importance.

The ability of Ca^{2+}/calmodulin to bind to the JM domain of EGFR(622−660) and remove it from the membrane extends the results we previously reported on the simpler JM domain peptide, EGFR(645−660) (*16*) and supports the extensive work of Villalobo and co-workers who first showed that EGFR binds Ca^{2+}/calmodulin (*53*−*55*).

The longer TM−JM peptide increases the biological relevance of our conclusions since the sequence is located between the extracellular ligand-binding and intracellular kinase domains, which are more thoroughly characterized. Two observations in the literature suggest that the JM region of the EGFR, as well as the activation loop in the kinase domain (*11*), is involved in autoinhibition.

First, membrane permeable Ca^{2+}/calmodulin inhibitors reduce the initial rate of EGFR trans autophosphorylation in several different cell types (*53*, *56*). It is known that EGF binding to EGFR leads to an initial burst in the intracellular Ca^{2+} concentration due to a transitory release of Ca^{2+} from intracellular stores (*3*) and that the resulting levels of Ca^{2+} are sufficient to activate calmodulin (*57*, *58*). Consequently, we propose that membrane permeable calmodulin inhibitors are effective in reducing EGFR activation during this period by inhibiting the formation of the active Ca^{2+}/calmodulin complex, which otherwise can bind to the JM region of EGFR(622−660) and release it from the membrane.

Second, membrane permeable weak bases (e.g., sphingosine) and increased salt concentrations (*59*, *60*) increase EGFR activity in the absence of EGF. For example, addition of 2 μM sphingosine, a membrane permeable weak base leads to increased receptor autophosphorylation (*42*). In Figure 8, we show that the addition of sphingosine is able to reduce FRET between Bodipy-TMR-PIP_2 and Texas-Red EGFR(622−660). We propose that disengaging the JM domain from the membrane surface (by binding of sphingosine to the bilayer, by salt decreasing electrostatic interactions, or by binding of Ca^{2+}/CaM to the JM region) releases one autoinhibition mechanism in the intact receptor and allows the kinase domains to associate as an asymmetric dimer and become activated through the allosteric mechanism described by Zhang et al. (*11*).

The Helical EGFR TM Domain Breaks at the TM−JM Boundary. The TM−JM region is sometimes viewed as a rigid rod that mechanically couples structural changes in the orientation of the extracellular domains to changes in the proximity and orientation of the kinase domains. For example, mutational studies provide evidence suggesting that the TM domain of the ErbB2 receptor is rotationally coupled to the orientation of the kinase domain (*17*) and that activation requires a specific rotational orientation of the monomers with respect to each other in the ErbB2 dimer (*61*).

If our observation that the helical TM domain breaks at the TM−JM boundary and that the JM domain is flexible can be extrapolated to the intact receptor, it challenges the rigid rod view of the TM−JM sequence. However, in the context of dimeric EGFR, association of the JM domain with the membrane surface establishes a defined orientation relative to the dimer interface. For instance, in the inactive dimer depicted in Figure 1 (right side), the JM sequences extend out from the TM dimer in opposite directions. Thus, binding to the membrane surface imposes an orientation on the extended, but unfolded or unstructured, JM sequence and may explain the observed dependence of receptor activation on the TM rotational orientation (*17*).

To address whether the TM helices in EGFR(622−660) have the potential to associate, deuterium magic angle spinning NMR measurements were made of specifically deuterated leucines in the TM sequence. Our observation of interactions between TM helices is consistent with the helix dimerization studies on the EGFR TM domains using the TOXCAT assay (*62*). On the basis of the maximum observed QCC (at Leu634), the helix−helix interaction is slightly weaker than that observed in the dimer of gp55-P TM helices. Such weak interactions may be mediated by an AxxxG motif in the C-terminal portion of the TM domain (*63*). Alanine and glycine have been found to have high propensities for mediating helix interactions in membrane proteins (*64*) and the C-terminal AxxxG motif is on the same face as Leu634 which exhibits the broadest deuterium line shape. The suggestion that Ala637 is in the preferred interface of EGFR-(622−660) is consistent with the observation that the C-terminal motif is involved in mediating homodimerization (*65*).

Weak interactions between TM domains may be sufficient to orient the TM helices when the receptor dimer is stabilized by ligand binding (*66*). Experiments are in progress to establish if there is an orientational dependence of the TM helices for Ca^{2+}/calmodulin binding to the JM sequence. An intriguing possibility is that there is electrostatic "charge matching" between the Ca^{2+}/calmodulin complex and the cytoplasmic JM domains when they are in close proximity in the EGFR dimer. The individual JM domains each have a charge of +8, while their combined charge of +16 exactly matches the net −16 charge of the Ca^{2+}/calmodulin complex. This may be important at high negative membrane surface potentials where the affinity of Ca^{2+}/calmodulin for the individual JM domains is not sufficient to pull it off the membrane. In this regard, we have shown that positively

charged peptides with no sequence homology to the EGFR JM region significantly increase the ability of Ca^{2+}/calmodulin to remove the JM peptide from membrane bilayers (unpublished results), probably by increasing the positive charge density in the vicinity of the JM peptide. Thus, dimerization or reorientation of existing dimers to bring two membrane-bound JM regions together may enhance the ability of Ca^{2+}/calmodulin to remove the JM region from the membrane and activate the EGFR, another possible biological example of "coincidence counting".

In summary, it is well established from structural studies of the extracellular domain that the initial step in the activation of the EGFR involves EGF-induced dimer formation (or dimer rearrangement). Zhang et al. (*11*) provide convincing evidence that the final step in the activation involves kinase−kinase dimer formation and an allosteric change in the conformation of the activation loop. Our work provides support for an intermediate step in the activation process that involves dissociation of the JM (and possibly kinase) domains from the membrane. The reversible dissociation of the JM region may be enhanced by binding of Ca^{2+}/calmodulin and would provide an additional layer of autoinhibition.

ACKNOWLEDGMENT

We gratefully acknowledge the W. M. Keck Foundation for support of the NMR facilities in the Center of Structural Biology at Stony Brook. We thank Xin Zhao for simulations of the deuterium MAS spectra.

NOTE ADDED AFTER ASAP PUBLICATION

The original posting of September 30, 2006 contained incorrect concentrations in the caption for Figure 2. The correct version is shown in the posting date of October 6, 2006.

REFERENCES

1. Schlessinger, J. (2000) Cell signaling by receptor tyrosine kinases, *Cell 103*, 211−225.
2. Hubbard, S. R. (2004) Juxtamembrane autoinhibition in receptor tyrosine kinases, *Nat. Rev. Mol. Cell Biol. 5*, 464−470.
3. Jorissen, R. N., Walker, F., Pouliot, N., Garrett, T. P. J., Ward, C. W., and Burgess, A. W. (2003) Epidermal growth factor receptor: mechanisms of activation and signalling, *Exp. Cell Res. 284*, 31−53.
4. Tiganis, T. (2002) Protein tyrosine phosphatases: Dephosphorylating the epidermal growth factor receptor, *IUBMB Life 53*, 3−14.
5. Carpenter, G. (2000) The EGF receptor: a nexus for trafficking and signaling, *Bioessays 22*, 697−707.
6. Le Roy, C., and Wrana, J. L. (2005) Clathrin- and non-clathrin-mediated endocytic regulation of cell signalling, *Nat. Rev. Mol. Cell Biol. 6*, 112−126.
7. Blume-Jensen, P., and Hunter, T. (2001) Oncogenic kinase signalling, *Nature 411*, 355−365.
8. Holbro, T., Civenni, G., and Hynes, N. E. (2003) The ErbB receptors and their role in cancer progression, *Exp. Cell Res. 284*, 99−110.
9. Ogiso, H., Ishitani, R., Nureki, O., Fukai, S., Yamanaka, M., Kim, J. H., Saito, K., Sakamoto, A., Inoue, M., Shirouzu, M., and Yokoyama, S. (2002) Crystal structure of the complex of human epidermal growth factor and receptor extracellular domains, *Cell 110*, 775−787.
10. Ferguson, K. M., Berger, M. B., Mendrola, J. M., Cho, H. S., Leahy, D. J., and Lemmon, M. A. (2003) EGF activates its receptor by removing interactions that autoinhibit ectodomain dimerization, *Mol. Cell 11*, 507−517.
11. Zhang, X., Gureasko, J., Shen, K., Cole, P. A., and Kuriyan, J. (2006) An allosteric mechanism for activation of the kinase domain of epidermal growth factor receptor, *Cell 125*, 1137−1149.
12. Hubbard, S. R. (2006) EGF receptor activation: Push comes to shove, *Cell 125*, 1029−1031.
13. Landau, M., Fleishman, S. J., and Ben-Tal, N. (2004) A putative mechanism for downregulation of the catalytic activity of the EGF receptor via direct contact between its kinase and C-terminal domains, *Structure 12*, 2265−2275.
14. Aifa, S., Aydin, J., Nordvall, G., Lundstrom, I., Svensson, S. P. S., and Hermanson, O. (2005) A basic peptide within the juxtamembrane region is required for EGF receptor dimerization, *Exp. Cell Res. 302*, 108−114.
15. Aifa, S., Miled, N., Frikha, F., Aniba, M. R., Svensson, S. P. S., and Rebai, A. (2006) Electrostatic interactions of peptides flanking the tyrosine kinase domain in the epidermal growth factor receptor provides a model for intracellular dimerization and autophosphorylation, *Proteins 62*, 1036−1043.
16. McLaughlin, S., Smith, S. O., Hayman, M. J., and Murray, D. (2005) An electrostatic engine model for autoinhibition and activation of the epidermal growth factor receptor (EGFR/ErbB) family, *J. Gen. Physiol. 126*, 41−53.
17. Bell, C. A., Tynan, J. A., Hart, K. C., Meyer, A. N., Robertson, S. C., and Donoghue, D. J. (2000) Rotational coupling of the transmembrane and kinase domains of the Neu receptor tyrosine kinase, *Mol. Biol. Cell 11*, 3589−3599.
18. Sato, T., Kawakami, T., Akaji, K., Konishi, H., Mochizuki, K., Fujiwara, T., Akutsu, H., and Aimoto, S. (2002) Synthesis of a membrane protein with two transmembrane regions, *J. Pept. Sci. 8*, 172−180.
19. Smith, S. O., Eilers, M., Song, D., Crocker, E., Ying, W. W., Groesbeek, M., Metz, G., Ziliox, M., and Aimoto, S. (2002) Implications of threonine hydrogen bonding in the glycophorin A transmembrane helix dimer, *Biophys. J. 82*, 2476−2486.
20. Liu, W., Crocker, E., Constantinescu, S. N., and Smith, S. O. (2005) Helix packing and orientation in the transmembrane dimer of gp55-P of the spleen focus forming virus, *Biophys. J. 89*, 1194−1202.
21. Gambhir, A., Hangyas-Mihalyne, G., Zaitseva, I., Cafiso, D. S., Wang, J. Y., Murray, D., Pentyala, S. N., Smith, S. O., and McLaughlin, S. (2004) Electrostatic sequestration of PIP2 on phospholipid membranes by basic/aromatic regions of proteins, *Biophys. J. 86*, 2188−2207.
22. Golebiewska, U., Gambhir, A., Hangyas-Mihalyne, G., Zaitseva, I., Rädler, J., and McLaughlin, S. (2006) Membrane-bound basic peptides sequester multivalent (PIP_2), but not monovalent (PS), acidic lipids, *Biophys. J. 91*, 588−599.
23. Metz, G., Wu, X., and Smith, S. O. (1994) Ramped-amplitude cross polarization in magic angle spinning NMR, *J. Magn. Reson. A 110*, 219−227.
24. Bennett, A. E., Rienstra, C. M., Auger, M., Lakshmi, K. V., and Griffin, R. G. (1995) Heteronuclear decoupling in rotating solids, *J. Chem. Phys. 103*, 6951−6958.
25. Bak, M., Rasmussen, J. T., and Nielsen, N. C. (2000) SIMPSON: A general simulation program for solid-state NMR spectroscopy, *J. Magn. Reson. 147*, 296−330.
26. Stamos, J., Sliwkowski, M. X., and Eigenbrot, C. (2002) Structure of the epidermal growth factor receptor kinase domain alone and in complex with a 4-anilinoquinazoline inhibitor, *J. Biol. Chem. 277*, 46265−46272.
27. van Dam, L., Karlsson, G., and Edwards, K. (2004) Direct observation and characterization of DMPC/DHPC aggregates under conditions relevant for biological solution NMR, *Biochim. Biophys. Acta-Biomembranes 1664*, 241−256.
28. Chen, Y. H., Yang, J. T., and Chau, K. H. (1974) Determination of the helix and β form of proteins in aqueous solution by circular dichroism, *Biochemistry 13*, 3350−3359.
29. Tamm, L. K., and Tatulian, S. A. (1997) Infrared spectroscopy of proteins and peptides in lipid bilayers, *Q. Rev. Biophys. 30*, 365−429.
30. Tjandra, N., and Bax, A. (1997) Large variations in $^{13}C_\alpha$ chemical shift anisotropy in proteins correlate with secondary structure, *J. Am. Chem. Soc. 119*, 9576−9577.
31. Saito, H., Tuzi, S., and Naito, A. (1998) Empirical versus nonempirical evaluation of secondary structure of fibrous and membrane proteins by solid-state NMR: A practical approach, *Annu. Rep. NMR Spectrosc. 36*, 79−121.

32. Rigby, A. C., Grant, C. W. M., and Shaw, G. S. (1998) Solution and solid state conformation of the human EGF receptor transmembrane region, *Biochim. Biophys. Acta 1371*, 241−253.
33. Siminovitch, D. J. (1998) Solid-state NMR studies of proteins: the view from static ^{2}H NMR experiments, *Biochem. Cell Biol. 76*, 411−422.
34. Ying, W. W., Irvine, S. E., Beekman, R. A., Siminovitch, D. J., and Smith, S. O. (2000) Deuterium NMR reveals helix packing interactions in phospholamban, *J. Am. Chem. Soc. 122*, 11125−11128.
35. Sharpe, S., Barber, K. R., and Grant, C. W. M. (2000) Val(659) → Glu mutation within the transmembrane domain of ErbB-2: Effects measured by ^{2}H NMR in fluid phospholipid bilayers, *Biochemistry 39*, 6572−6580.
36. Batchelder, L. S., Sullivan, C. E., Jelinski, L. W., and Torchia, D. A. (1982) Characterization of leucine side-chain reorientation in collagen-fibrils by solid-state 2H NMR, *Proc. Natl. Acad. Sci. U.S.A. 79*, 386−389.
37. Jones, D. H., Rigby, A. C., Barber, K. R., and Grant, C. W. M. (1997) Oligomerization of the EGF receptor transmembrane domain: A ^{2}H NMR study in lipid bilayers, *Biochemistry 36*, 12616−12624.
38. Rigby, A. C., Barber, K. R., Shaw, G. S., and Grant, C. W. M. (1996) Transmembrane region of the epidermal growth factor receptor: behavior and interactions via ^{2}H NMR, *Biochemistry 35*, 12591−12601.
39. Jones, D. H., Barber, K. R., and Grant, C. W. M. (1998) Sequence-related behaviour of transmembrane domains from class I receptor tyrosine kinases, *Biochim. Biophys. Acta 1371*, 199−212.
40. McLaughlin, S., and Murray, D. (2005) Plasma membrane phosphoinositide organization by protein electrostatics, *Nature 438*, 605−611.
41. Cho, W. H., and Stahelin, R. V. (2005) Membrane-protein interactions in cell signaling and membrane trafficking, *Annu. Rev. Biophys. Biomol. Struct. 34*, 119−151.
42. Davis, R. J., Girones, N., and Faucher, M. (1988) Two alternative mechanisms control the interconversion of functional states of the epidermal growth factor receptor, *J. Biol. Chem. 263*, 5373−5379.
43. Hunter, T., Ling, N., and Cooper, J. A. (1984) Protein kinase-C phosphorylation of the EGF receptor at a threonine residue close to the cytoplasmic face of the plasma-membrane, *Nature 311*, 480−483.
44. Cochet, C., Gill, G. N., Meisenhelder, J., Cooper, J. A., and Hunter, T. (1984) C-kinase phosphorylates the epidermal growth-factor receptor and reduces its epidermal growth factor-stimulated tyrosine protein kinase activity, *J. Biol. Chem. 259*, 2553−2558.
45. Wybenga-Groot, L. E., Baskin, B., Ong, S. H., Tong, J. F., Pawson, T., and Sicheri, F. (2001) Structural basis for autoinhibition of the EphB2 receptor tyrosine kinase by the unphosphorylated juxtamembrane region, *Cell 106*, 745−757.
46. Griffith, J., Black, J., Faerman, C., Swenson, L., Wynn, M., Lu, F., Lippke, J., and Saxena, K. (2004) The structural basis for autoinhibition of FLT3 by the juxtamembrane domain, *Mol. Cell 13*, 169−178.
47. Choowongkomon, K., Hobert, M. E., He, C., Carlin, C. R., and Sonnichsen, F. D. (2004) Aqueous and micelle-bound structural characterization of the epidermal growth factor receptor juxtamembrane domain containing basolateral sorting motifs, *J. Biomol. Struct. Dyn. 21*, 813.
48. Choowongkomon, K., Carlin, C. R., and Sonnichsen, F. D. (2005) A structural model for the membrane-bound form of the juxtamembrane domain of the epidermal growth factor receptor, *J. Biol. Chem. 280*, 24043.
49. Ullrich, A., Coussens, L., Hayflick, J. S., Dull, T. J., Gray, A., Tam, A. W., Lee, J., Yarden, Y., Libermann, T. A., Schlessinger, J., Downward, J., Mayes, E. L. V., Whittle, N., Waterfield, M. D., and Seeburg, P. H. (1984) Human epidermal growth-factor receptor cDNA sequence and aberrant expression of the amplified gene in A431 epidermoid carcinoma-cells, *Nature 309*, 418−425.
50. Berridge, M. J., and Irvine, R. F. (1984) Inositol trisphosphate, a novel 2nd messenger in cellular signal transduction, *Nature 312*, 315−321.
51. Czech, M. P. (2000) PIP2 and PIP3: Complex roles at the cell surface. *Cell 100*, 603−606.
52. McLaughlin, S., Wang, J. Y., Gambhir, A., and Murray, D. (2002) PIP2 and proteins: Interactions, organization, and information flow. *Annu. Rev. Biophys. Biomol. Struct. 31*, 151−175.
53. Li, H. B., Ruano, M. J., and Villalobo, A. (2004) Endogenous calmodulin interacts with the epidermal growth factor receptor in living cells. *FEBS Lett. 559*, 175−180.
54. Li, H. B., and Villalobo, A. (2002) Evidence for the direct interaction between calmodulin and the human epidermal growth factor receptor. *Biochem. J. 362*, 499−505.
55. Martin-Nieto, J., and Villalobo, A. (1998) The human epidermal growth factor receptor contains a juxtamembrane calmodulin-binding site. *Biochemistry 37*, 227−236.
56. Li, H. B., Sanchez-Torres, J., del Carpio, A., Salas, V., and Villalobo, A. (2004) The ErbB2/Neu/HER2 receptor is a new calmodulin-binding protein, *Biochem. J. 381*, 257−266.
57. Hughes, A. R., Bird, G. S. J., Obie, J. F., Thastrup, O., and Putney, J. W. (1991) Role of inositol (1,4,5)trisphosphate in epidermal growth factor-induced Ca2+ signaling in A431-cells, *Mol. Pharmacol. 40*, 254.
58. Nojiri, S., and Hoek, J. B. (2000) Suppression of epidermal growth factor-induced phospholipase C activation associated with actin rearrangement in rat hepatocytes in primary culture, *Hepatology 32*, 947.
59. King, C. R., Borrello, I., Porter, L., Comoglio, P., and Schlessinger, J. (1989) Ligand-independent tyrosine phosphorylation of Egf receptor and the Erbb-2/Neu proto-oncogene product is induced by hyperosmotic shock, *Oncogene 4*, 13−18.
60. Rodriguez, I., Kaszkin, M., Holloschi, A., Kabsch, K., Marques, M. M., Mao, X., and Alonso, A. (2002) Hyperosmotic stress induces phosphorylation of cytosolic phospholipase A(2) in HaCaT cells by an epidermal growth factor receptor-mediated process, *Cell Signal 14*, 839−848.
61. Cao, H., Bangalore, L., Bormann, B. J., and Stern, D. F. (1992) A subdomain in the transmembrane domain is necessary for p185neu* activation, *EMBO J. 11*, 923−932.
62. Mendrola, J. M., Berger, M. B., King, M. C., and Lemmon, M. A. (2002) The single transmembrane domains of ErbB receptors self- associate in cell membranes, *J. Biol. Chem. 277*, 4704−4712.
63. Fleishman, S. J., Schlessinger, J., and Ben-Tal, N. (2002) A putative molecular-activation switch in the transmembrane domain of erbB2, *Proc. Natl. Acad. Sci. U.S.A. 99*, 15937−15940.
64. Eilers, M., Patel, A. B., Liu, W., and Smith, S. O. (2002) Comparison of helix interactions in membrane and soluble α-bundle proteins, *Biophys. J. 82*, 2720−2736.
65. Gerber, D., Sal-Man, N., and Shai, Y. (2004) Two motifs within a transmembrane domain, one for homodimerization and the other for heterodimerization, *J. Biol. Chem. 279*, 21177−21182.
66. Stanley, A. M., and Fleming, K. G. (2005) The transmembrane domains of ErbB receptors do not dimerize strongly in micelles, *J. Mol. Biol. 347*, 759−772.

BI061264M